62-1-4

XEROX

MODEL STUDIES OF SEISMIC ENERGY DISTRIBUTION AROUND DIFFERENT TYPES OF SOURCE

B.F. Howell, Jr.
P.M. Lavin
J.H. Pfluke

The Pennsylvania State University
Department of Geophysics and Geochemistry
Mineral Sciences Building
University Park, Pennsylvania
814-UN 5-6821 and 814-UN 5-2622

Progress Report No. 4

Contract AF19(604)-7383
(expires 31 August 1962)

30 November 1961

Prepared
for

GEOPHYSICS RESEARCH DIRECTORATE
AIR FORCE CAMBRIDGE RESEARCH LABORATORIES
OFFICE OF AEROSPACE RESEARCH
UNITED STATES AIR FORCE
BEDFORD, MASSACHUSETTS

WORK SPONSORED BY ADVANCED RESEARCH PROJECTS AGENCY

PROJECT VELA-UNIFORM

ARPA Order No. 180-61, Amendment 2

Project Code No. 8100, Task 2

MODEL STUDIES OF SEISMIC ENERGY DISTRIBUTION AROUND DIFFERENT TYPES OF SOURCE

Progress Report No. 4
for the quarter ending November 30, 1961

I. SIMULATED MODEL

One of the objectives of this research has been to accumulate a "library" of pictures showing the patterns of first motion around different types of source as a function of azimuth for a uniform medium. The gathering of data for this purpose has now been completed. Data on first shear (S) waves under the same conditions has also been recorded. Four source systems simulating an explosion, a simple unidirectional force, a single couple and a double couple have been modeled.

The patterns are modified in the presence of velocity discontinuities near the source. Five typical conditions have been studied: a boundary passing thru the focus; one to one side of the focus; two boundaries symmetrically on either side of the focus; a similar arrangement with the two boundaries assymetrical; and a circular area of higher velocity to one side of the fault. A complete set of records for both P and S waves has been obtained for the six different models for each of the four source systems under study. This is by no means all the cases which could be studied profitably, but it does serve to illustrate the type of result to be expected.

Evaluation of the P-wave data is well under way. To date, the shear-wave records have been studied only for the homogeneous model. Table I summarizes the present status of the analysis of the records. An evaluation of this data will complete phase I of the proposed research and will be prepared as a report for presentation before a professional society and for publication. Further experiments may be directed at specific special cases differing from the general cases covered here.

Preliminary Results:

In general, the results in the uniform models are consistant with theory. The amplitudes and directions of first motion for the compressional waves for all uniform models and for the shear waves for two uniform models were presented in earlier reports. The basic patterns for the shear waves for the double-couple and radial-force models in a uniform disc are shown in Fig. 1.

The strength of the shear wave was found to be greater than that of the compressional wave for all the uniform models except in the case of the radial force. For the single force and double couple, the maximum amplitude of S is about two times as strong as the maximum P. For the single couple, maximum S is about four times as strong as P. In the case of the radial force, the amplitude of S is very small compared to the average value for P. Also, from setting up numerous radial-force models, it appears that the smaller the scatter in P-wave amplitudes with azimuth,

the smaller the S-wave amplitudes for the uniform model. There appears to be a definite correlation between the overall assymmetry in the P-wave amplitudes and the generation of the S-waves.

The remainder of the S-wave data will be discussed at a later date. Difficulties have been encountered in the interpretation of the S-wave first motions for the non-uniform models due to the presence of energy arriving just before and during the arrival of the main shear pulse. This problem is also encountered in the interpretation of actual earthquake seismograms.

The peak amplitudes for the compressional waves in the four uniform models were measured. A consistency was found to exist between the first, second and third peaks. This is illustrated for the case of the single force in Fig. 2. In the upper graph the relative values of the first four peaks are plotted, a positive value indicating up on the record (away from source on model). The amplitudes of the fourth peaks are not consistent with the second peaks due in part to the simultaneous arrival of a new phase. The lower graph shows the normalized peak-to-peak value for the first two peaks (P_{1-2}) and the second and third peaks (P_{2-3}). The S-wave data will be studied in a similar fashion as will all the data for the non-uniform models.

The presence of the various velocity discontinuities have not, except in one case, reversed the direction of first motion of the P wave. This is illustrated for three models for the case of the single-couple and radial-force systems in Figs. 3 and 4, respectively. The solid curves in Fig. 3 are the theoretical curves for the P-wave distribution for the uniform single-couple model.

Reversals of the first motion of P compared to the theoretical direction for the uniform model are present in one model over a limited azimuthal range at the boundary of the velocity discontinuity (Fig. 5). This model had a double-couple source with a velocity discontinuity running through the source parallel to a shear plane. The reversals appear to be due to the initial arrival of a refracted wave of opposite sign from that of the direct wave at points within 30 degrees of the boundary in the low-velocity zone.

In the cases of the single- and double-couple models there appears to be a shifting of the nodal points in the low-velocity channel of less than 15 degrees toward one boundary of the high-velocity medium.

The effect of a boundary of any kind is to reduce the amplitudes of the P waves received in the high-velocity medium and in some cases in the shadow of the high-velocity zone. There is a sudden decrease in amplitude upon crossing the velocity discontinuity into the high-velocity medium as can be seen in Figs. 3 and 4. Records obtained on the

boundary may exhibit normal or reduced amplitudes depending on whether the pick-up transducer overlaps more of the low- or of the high-velocity medium. A quantitative analysis of the amount of reduction in amplitudes to be expected, due to the presence of the boundary and the difference in elastic properties of the two media, will be made later.

II. ACTUAL-DISPLACEMENT EXPERIMENTS

Frozen-fault:

Figure 6 shows a graph of some relative amplitudes of the P wave for the actual-displacement model. The records corresponding to these data were obtained in the manner described on page 9 of Progress Report No. 3. The azimuths falling within the shaded areas correspond to azimuths which are shielded from direct radiation from the source by slits (refer to to Fig. 2 of Progress Report No. 3 for geometry of the source region). The cosine curve superposed on the data is that of the theoretical relative amplitudes to be expected from a single-force source. The data for the azimuths 0-180° might be expected to follow this theoretical curve more closely than any other because the slits block radiation from the tongue side of the model.

Examination of the graph will reveal that the data do not follow this theoretical curve closely. Although dilatation might be expected in the 90-180° region, compressions are observed at all azimuths. The reason for this has not been determined.

Mechanically displaced fault:

The results over the past months obtained using the frozen-fault technique have not been entirely satisfactory and the method is very time consuming. In an effort to accellerate the accummulation of data, other techniques have been attempted which do not require freezing. One technique which shows considerable promise employs the same type of model and electrical circuitry as has been heretofore used, but stress is applied simply by inserting a blade into one of the slits of the model and twisting it manually. The fault surfaces, being in tight contact resist slipping because of static friction. Stress builds up on both sides of the fault. When the static friction is finally overcome, the fault surfaces move suddenly, thus releasing part of the stress in the form of elastic waves.

Records of the radial component at 5 azimuths made by the new technique are shown in Fig. 7. There is a clear similarity between these records and those made by the frozen-fault technique (refer to Fig. 11, Progress Report No. 3). The P-wave first motion appears as a distinct pulse in both cases. There is also a strong long-period component associated with the records made using both techniques. Reproducibility of records is shown for two azimuths in Fig. 7.

Figure 8A shows examples of "double breaks", a phenomenon that is also prevalent in the frozen-fault records. In this case the stress is released in a

series of steps resulting in overlapping wave trains (see discussion on page 3 of Quarterly Report No. 2, fourth paragraph).

The records of the two methods also differ in some respects. Although the wave trains appear the same, the plots of direction of first-motion against azimuth do not appear to follow the same pattern. P-wave motions for the frozen-fault were compressed at all azimuths, whereas the new technique yields compressions in the range 0-90° and dilation from 90-180°. The latter distribution is consistent with the hypothesis that the source mechanism is equivalent to a single force.

Radial component records using the new technique have been made at 15° intervals around the model. First-motion relative amplitudes have been plotted in Figure 9. The theoretical curve for the single-force source has been superposed on this plot. For azimuths 0-180° the directions of first motion agree with the hypothetical curve, but amplitudes are widely scattered about the curve. For azimuths 180-360° the directions of first motion do not always agree with the hypothetical curve. This is not surprising since most of the recording azimuths in this half of the model are shielded by the slits from the direct P wave. Also, the presence of the slits will cause stress concentrations which could be expected to alter the first-motion pattern appreciably. Another difficulty which is

encountered at many azimuths from 180-360° is the first motion is not a clean pulse, but rather appears to be made up of a multiplicity of pulses. The interference of these pulses makes interpretation of amplitudes at these azimuths ambiguous. A sample record demonstrating this interference effect is shown in Fig. 8B.

TABLE I

Present Status of Evaluation of Simulated Model Data

		Single Force	Single Couple	Double Couple	Radial Force
1. Uniform Model					
(1st P-wave peak)	P_1	P	P	P	P
(1st shear peak)	S_1^1	P	P	N	N
(2nd and 3rd P)	P_2^1, P_3	N	R	R	R
2. 1/2 Aluminum model					
(1st P)	P_1	R	P	R	P
(1st shear)	S_1^1	F	F	F	F
(2nd and 3rd P)	P_2^1, P_3	R	F	F	F
3. 3/8 Aluminum model					
(1st P)	P_1	R	N	R	N
(1st shear)	S_1^1	F	F	F	F
4. 3/2 low-velocity zone					
(1st P)	P_1	R	R	R	R
(1st shear)	S_1^1	F	F	F	F
(2nd and 3rd P)	P_2^1, P_3	R	R	F	F
5. 3/3 low-velocity zone					
(1st P)	P_1	R	N	R	N
(1st shear)	S_1^1	F	F	F	F
(2nd and 3rd P)	P_2^1, P_3	R	F	F	F
6. Spot					
(1st P)	P_1	R	N	R	N
(1st shear)	S_1^1	F	F	F	F

key: P = in a previous report
N = in this report
R = studied but not presented
F = records made but not interpreted

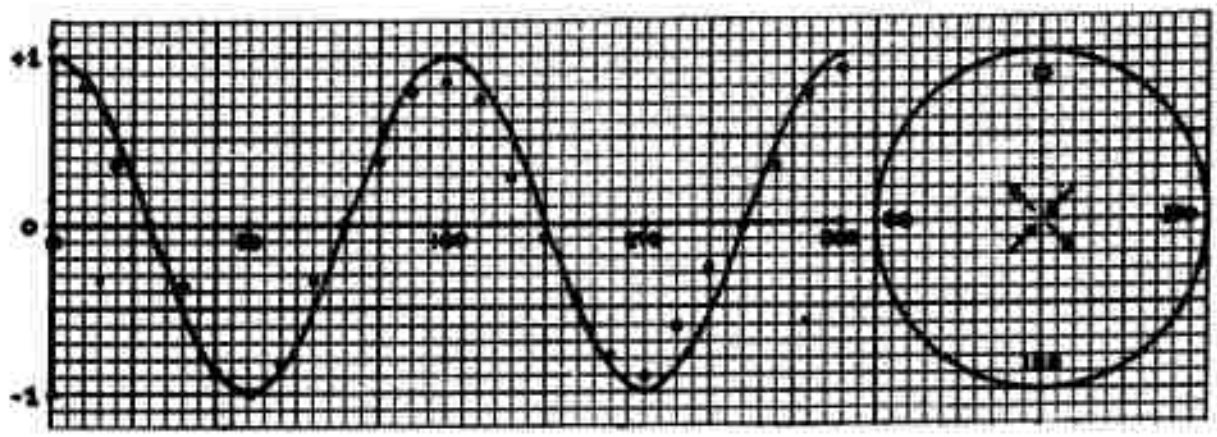

Fig. 1A. Theoretical (solid curve) and observed shear-wave amplitudes for the double-couple source shown at the right.

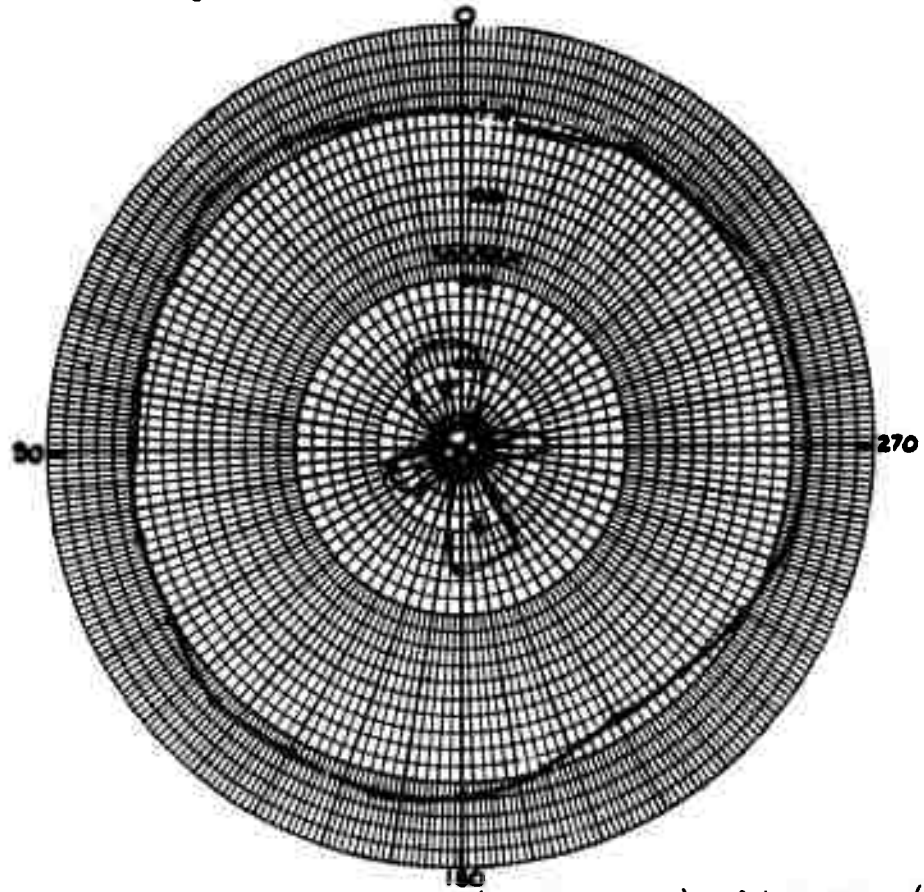

Fig. 1B. Observed amplitudes of radial (P, outer curve) and transverse (S, inner curve, + indicates clockwise motion) motions for a radial-force source.

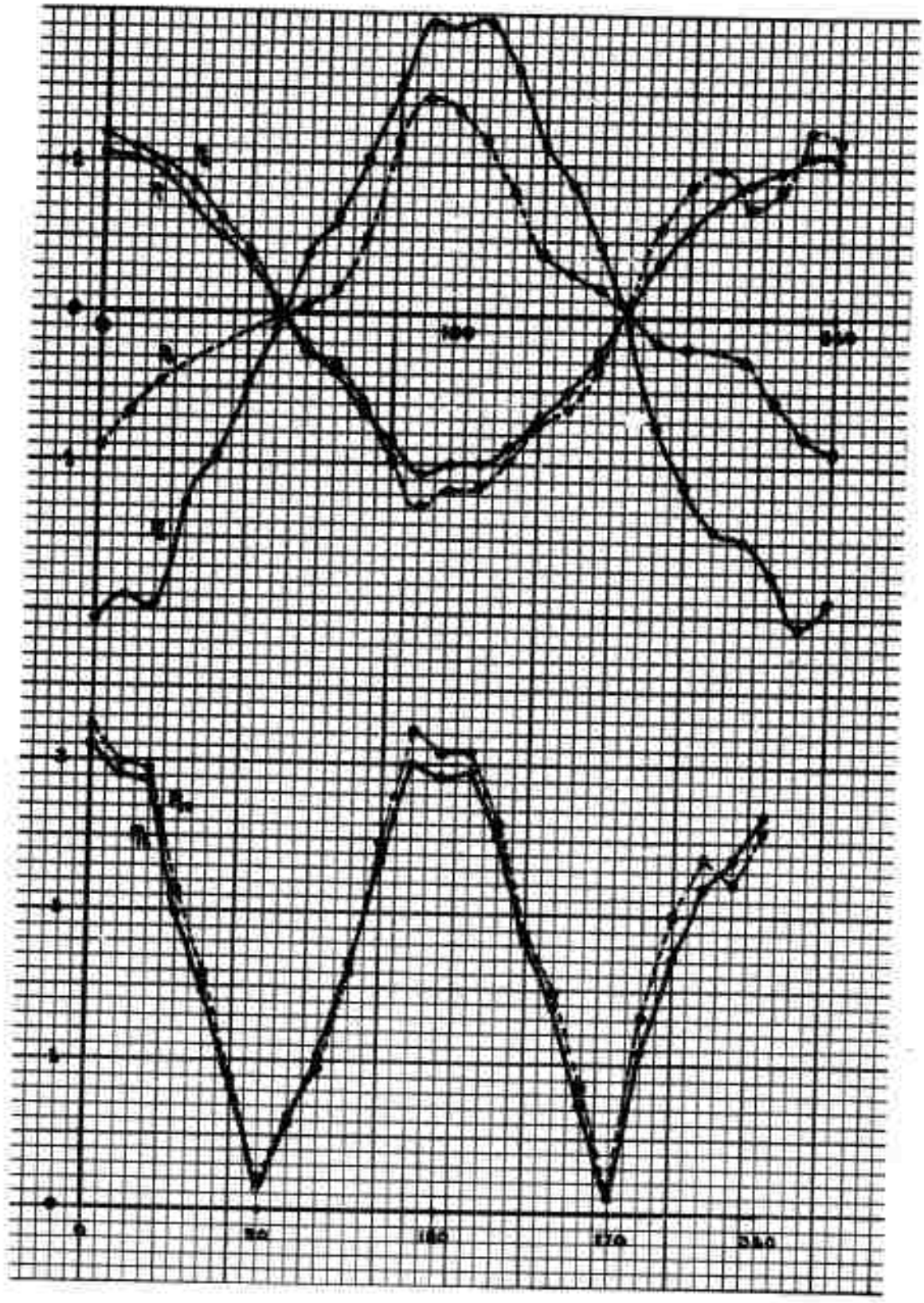

Fig. 2. Upper curve: relative strengths of first four P-wavespeaks for the single-force source. Lower curve: peak-to-peak amplitudes for the first-to-second (P_{12}) and second-to-third (P_{23}) peaks.

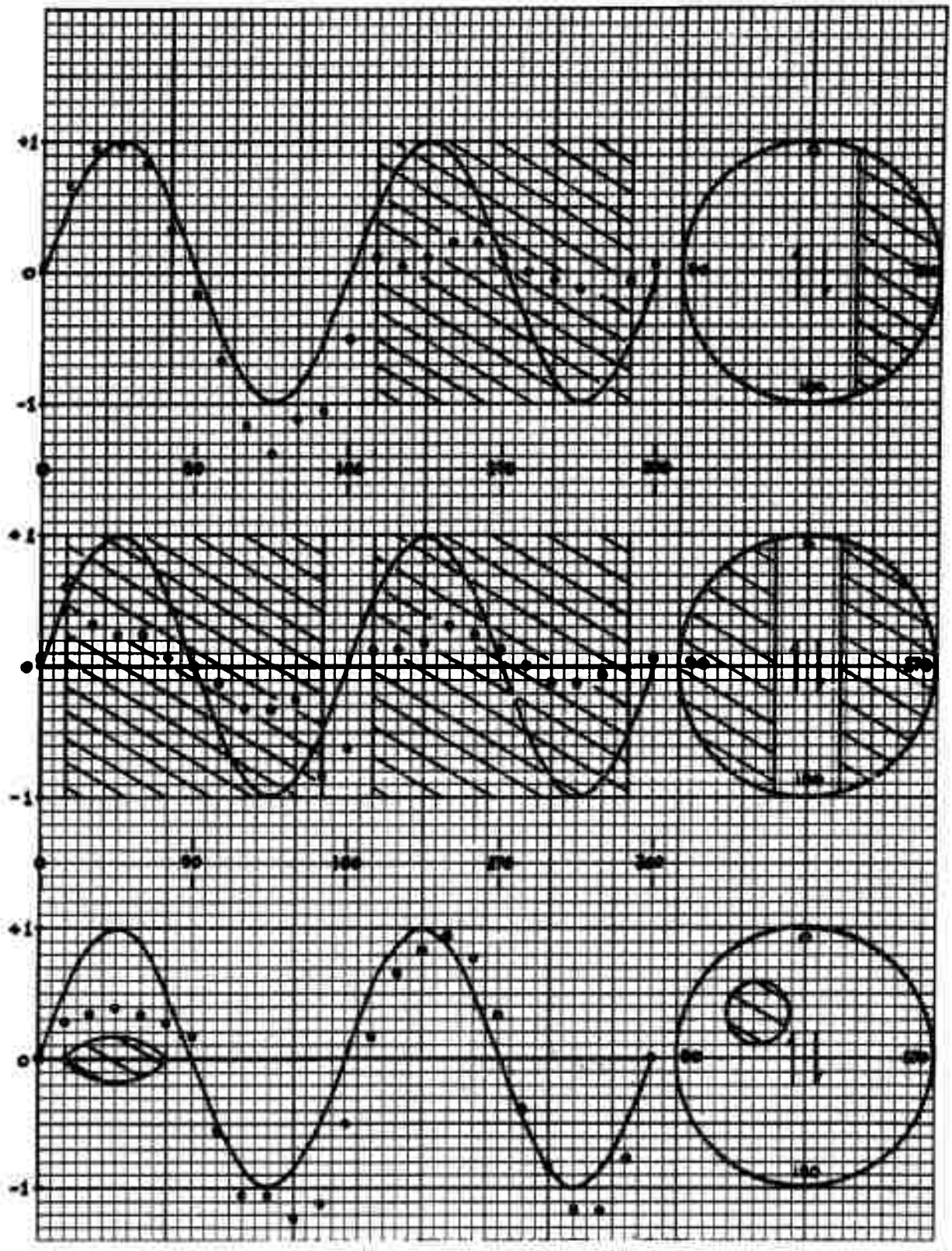

Fig. 3. Observed P-wave amplitudes for the three non-uniform models shown, single-couple source. Corresponding theoretical curve for the uniform model is shown for comparison. Shaded areas represent the high-velocity sections.

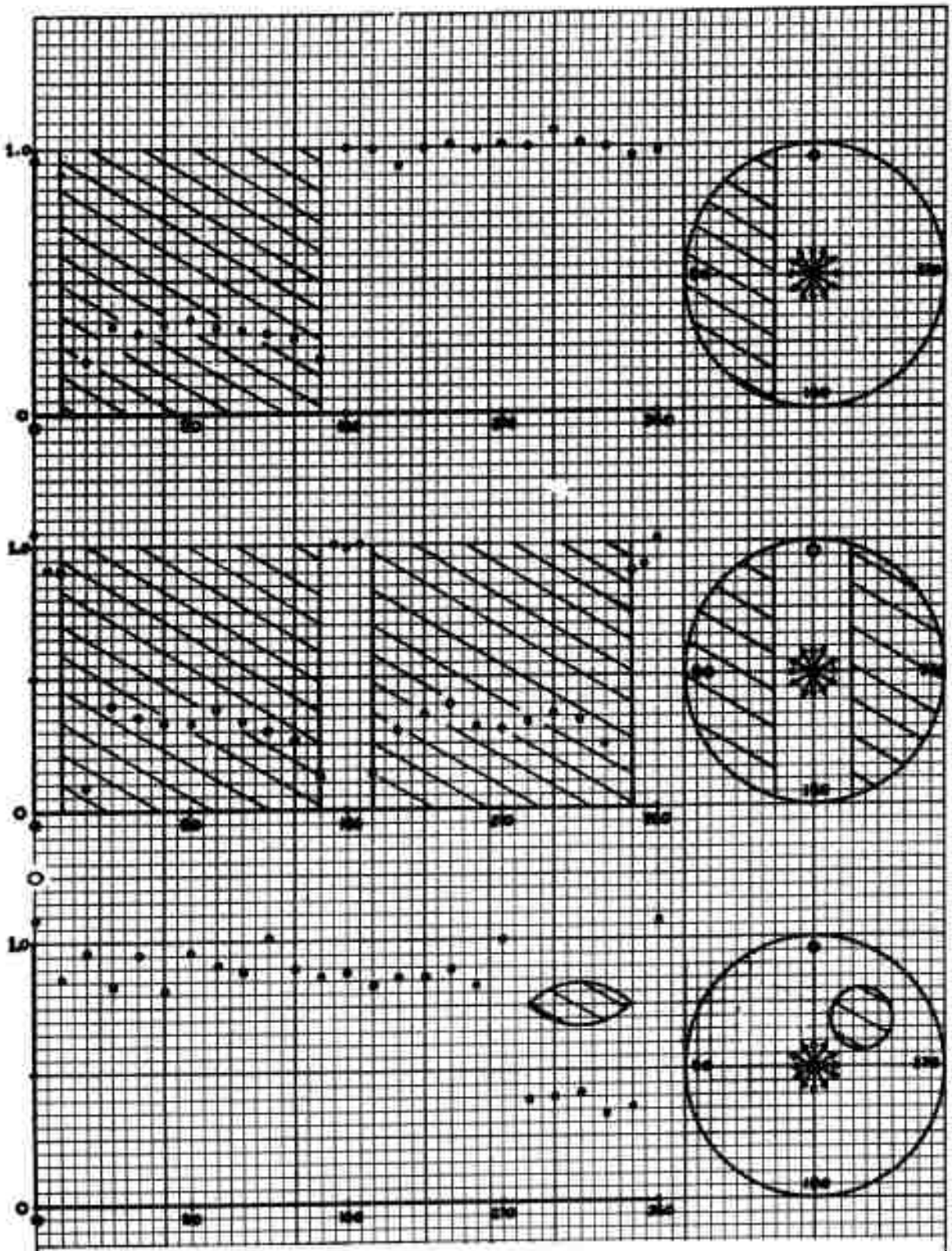

Fig. 4. Observed P-wave amplitudes for the three non-uniform models shown, radial-force source. Shaded areas represent the high-velocity sections.

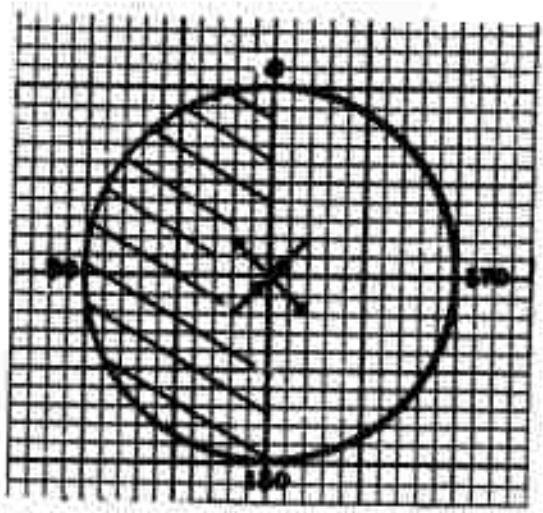

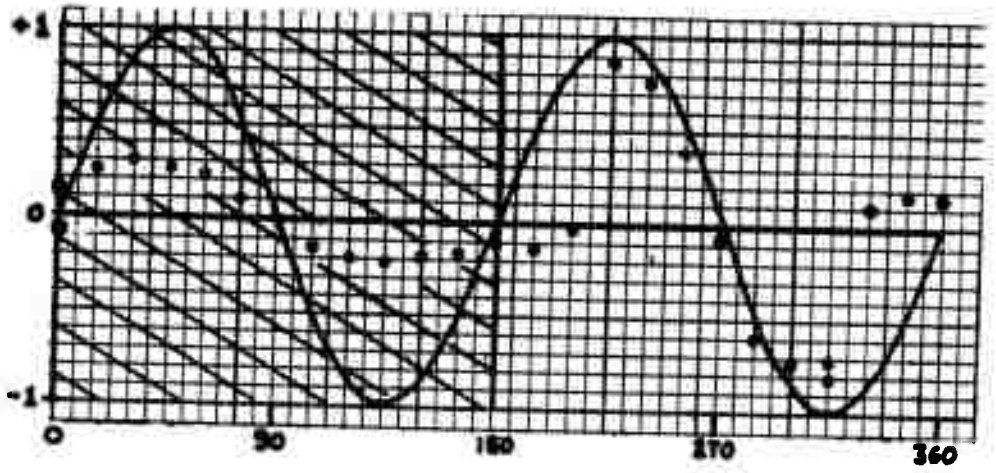

Fig. 5. Observed P-wave amplitudes in the presence of a velocity discontinuity, double-couple source. Theoretical curve for uniform model is shown for comparison. Shaded area represents the high-velocity section.

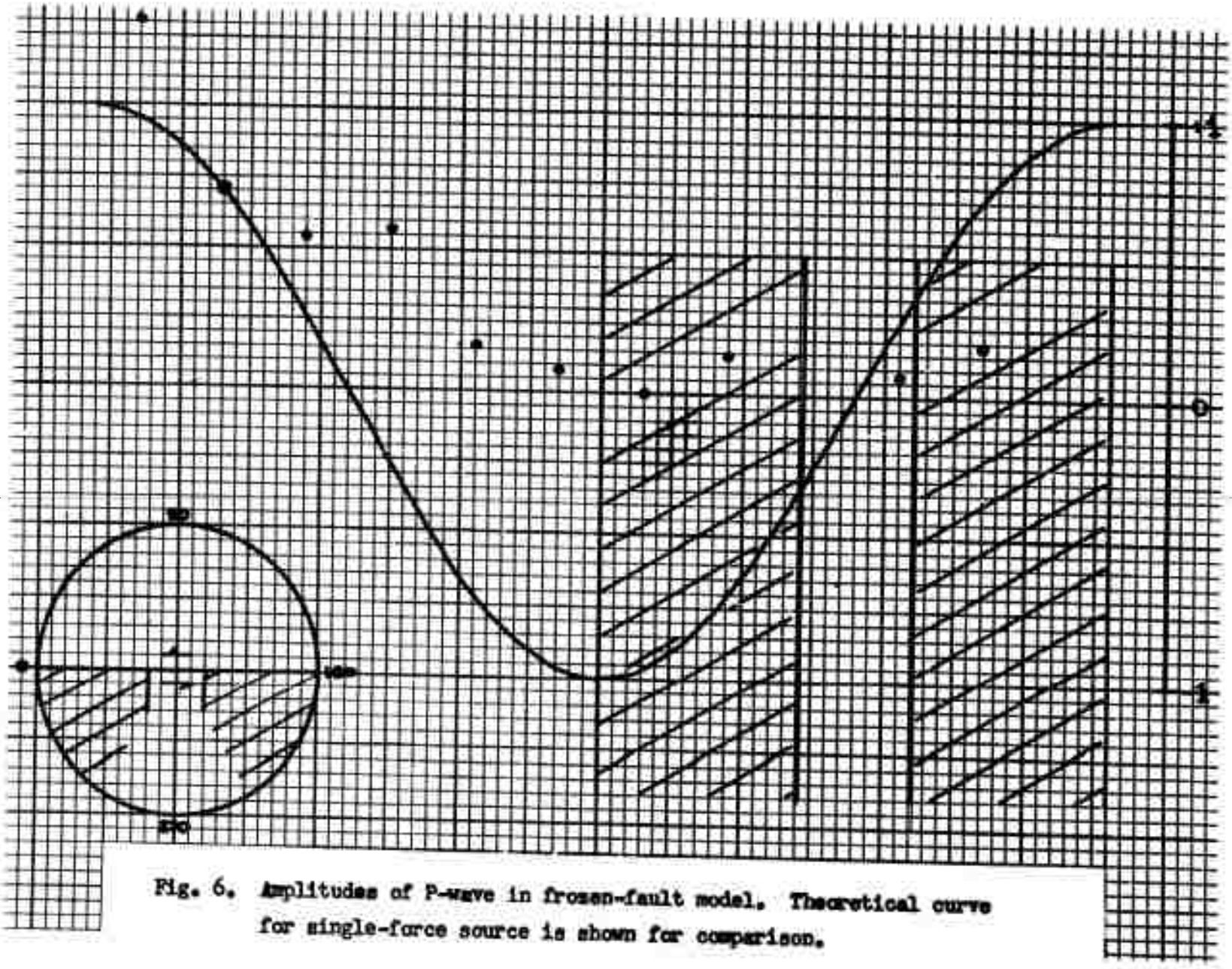

Fig. 6. Amplitudes of P-wave in frozen-fault model. Theoretical curve for single-force source is shown for comparison.

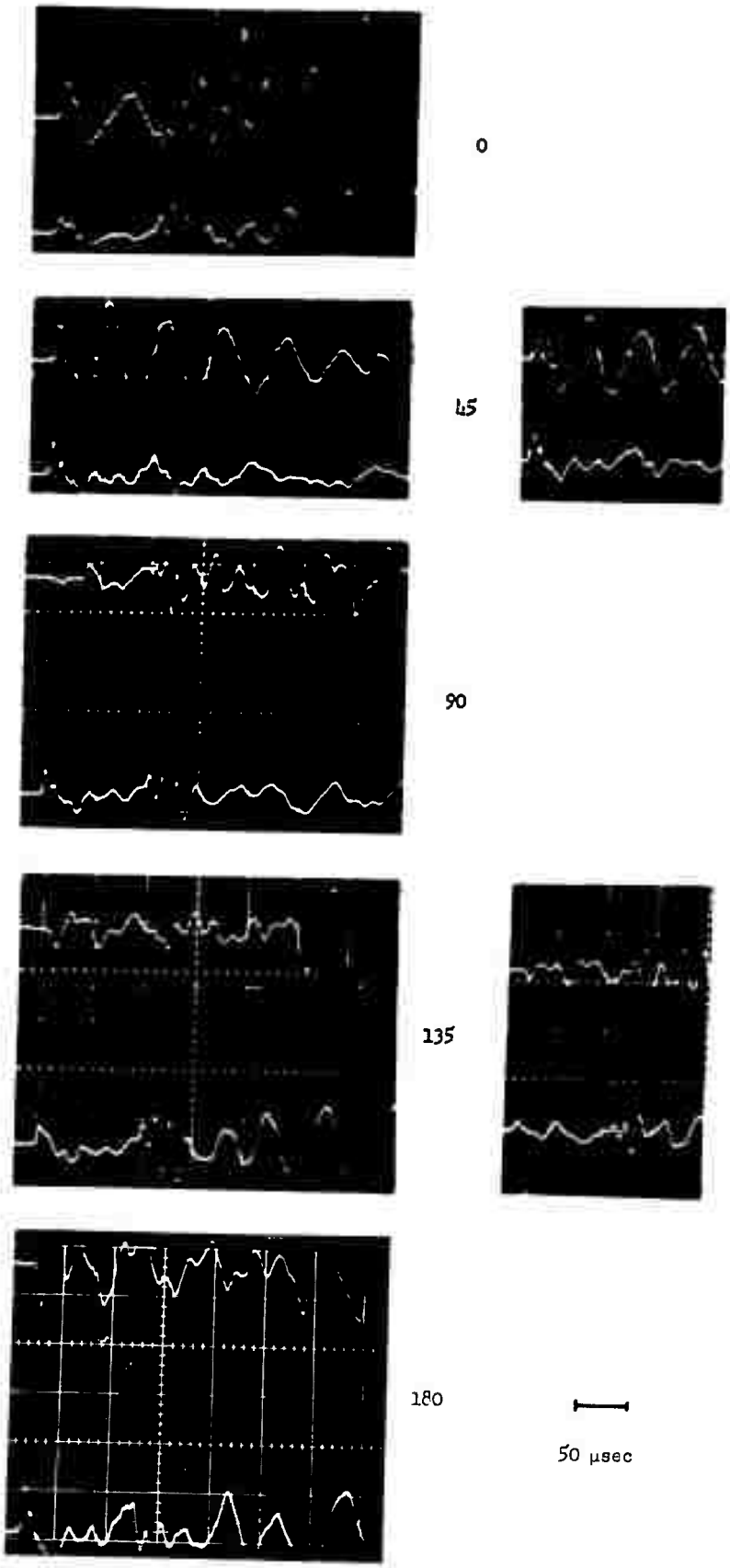

Fig. 7. Records at five azimuths for mechanically displaced fault.

Fig. 8a: Double breaks

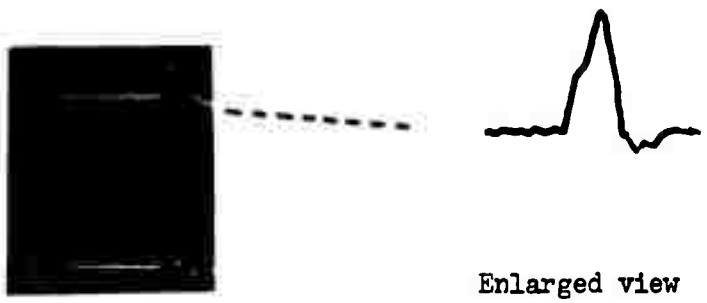

Fig. 8b: First break consisting of two overlapping pulses

Fig. 8: Records of compound pulses

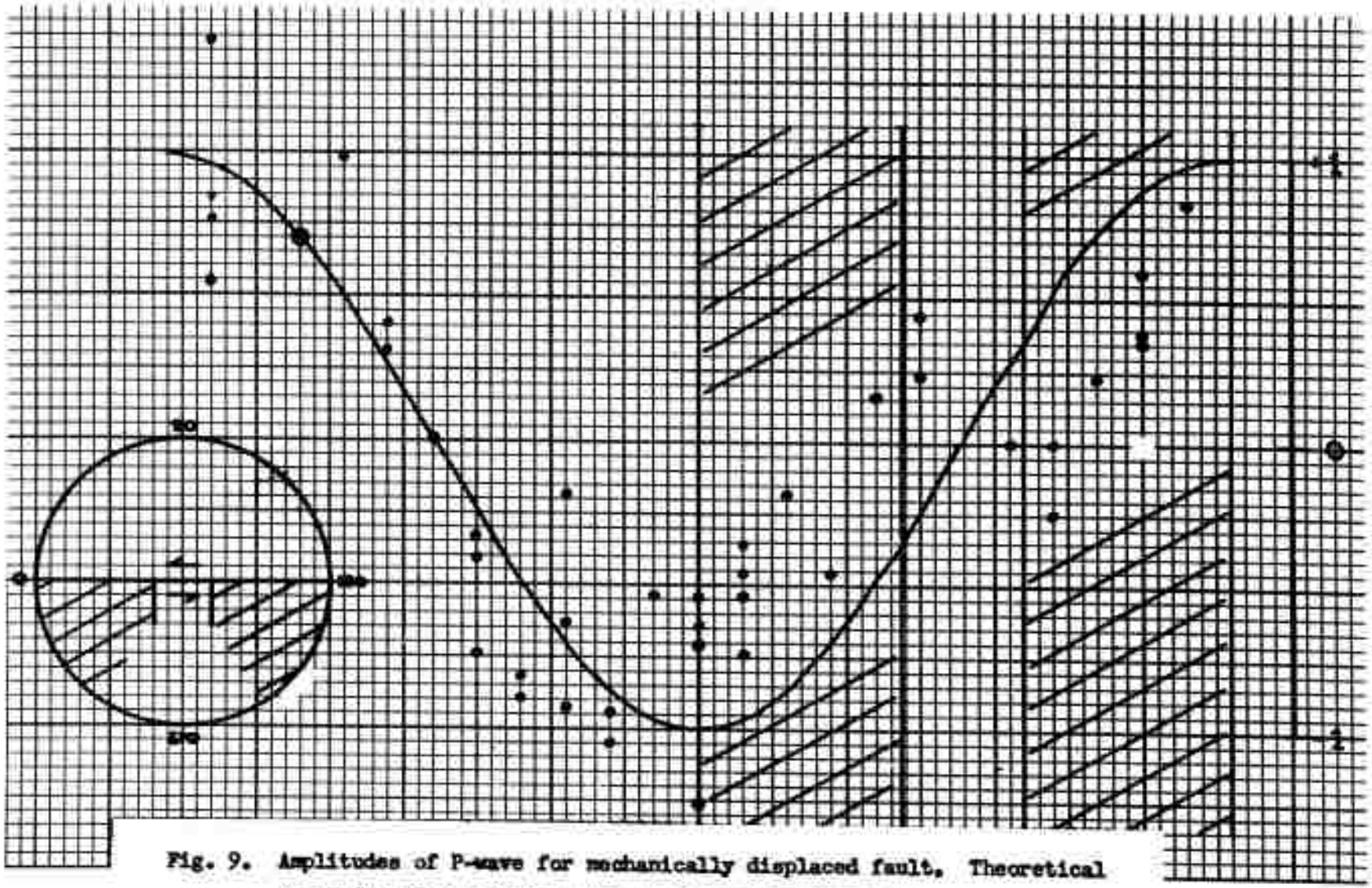

Fig. 9. Amplitudes of P-wave for mechanically displaced fault. Theoretical curve for single-force source is shown for comparison.

UNCLASSIFIED